Design of 71-76 GHz Double Corrugated Waveguide Traveling Wave Tube for Satellite Downlink

Xiang Li, Xuejiao Huang, Storm Mathisen, Rosa Letizia, *IEEE Member*, Claudio Paoloni, *IEEE Senior Member*

***Abstract*— The growing interest in wireless high data rate communications at millimeter waves both for terrestrial networks and satellite communications is stimulating novel solutions to overcome the strong atmosphere attenuation. In particular, the development of high throughput satellite communication systems for internet distribution is fundamental to complement the terrestrial networks and to cover regions not connected to terrestrial backbones, such as sea or remote areas. Ku-band and Ka-band satellite systems are presently available. Recently, the W-band (71 -76 GHz, 81-86 GHz) has been allocated for multigigabit transmissions, providing 5 GHz bandwidth both for uplink and downlink. However, it has been estimated that for enabling high throughput W-band satellite communication systems, transmission power higher than 50 W is needed. In this paper, a 71-76 GHz double corrugated waveguide (DCW) traveling wave tube (TWT) is designed as amplifier for high-data rate satellite downlink, with about 70 W output power. The dispersion characteristic of the designed DCW is experimentally validated by cold test. The proposed TWT is also a test vehicle, scaled in frequency, for a future novel 220 GHz DCW TWT for terrestrial wireless networks.**

***Index Terms*—Double corrugated waveguide, Traveling wave tube, Satellite communications, W-band.**

I. Introduction

GLOBALLY, mobile data traffic is predicted to grow 7-fold between 2016 and 2021, amounting to 49 exabytes per month by 2021 [1]. Such data growth already makes the actual terrestrial networks insufficient for future wireless communications, requiring new architectures and solutions. High data rate satellite communications are considered a complementary solution to terrestrial networks. Satellites are also used to cover regions not connected to optical fiber backbones such as sea and remote areas, or to provide resilience to the terrestrial networks in extreme circumstances, such as natural disasters. To date, the satellite systems at Ka-band and Ku-band provide data rate up to 150 Gbps. Nevertheless, the high throughput demand makes the actual provision insufficient. Recently, the W-band, 71-76 GHz for the downlink and 81-86 GHz for the uplink, has been allocated for multi-gigabit transmission [2]-[4]. This has raised a relevant interest in high data rate satellites at W-band [3]. However, the high atmosphere attenuation due to gases, rain and clouds is a strong obstacle for propagation, especially when 99.99% availability is required. As a result, the estimation of the link budget to support high modulation orders suggests values of transmission power above 50 W [5 - 6].

Traveling wave tubes (TWTs) are presently the only compact devices able to provide wideband high-power amplification with tens of watt at millimeter waves [7-8]. Reliability, robustness against high thermal stress and high saturated power make TWTs the preferred devices in the majority of airborne and space applications. Conventional space TWTs are based on the helix slow-wave structure (SWS), which can provide multi-octave bandwidths and output powers above 100 W up to 50 - 60 GHz [8-11]. The dimensions of a helix SWS inversely scale with the operation frequency, making its fabrication and alignment extremely demanding at the increase of the frequency, if not impossible above 70 GHz. The W-band is an upper limit for helix fabrication. Therefore, at the increase of the frequency, different slow wave structures, suitable to be fabricated by modern microfabrication techniques, are needed to build TWTs for enabling future constellations of high capacity W-band satellites [12] - [16].

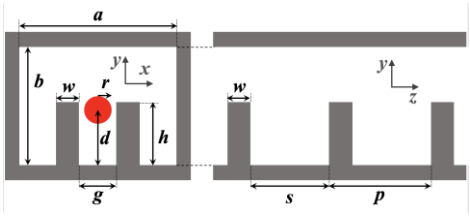

Fig. 1. Schematic of the DCW transverse and axial cross-sections.

Among these, the Double Corrugated Waveguide (DCW) was conceived as easy assembly SWS for millimeter waves tubes [16]-[17]. It supports a pencil electron beam flowing between two rows of pillars, enclosed in a rectangular waveguide (Fig. 1). The DCW is broadband, simple to build, robust and compatible with advanced fabrication techniques including UV-LIGA (German acronym of lithography, electroplating and molding) process [18] and high-precision CNC milling, being cost-effective and with high yield.

Manuscript received in 2017. (Corresponding Author: Claudio Paoloni.).
Xiang Li, Xuejiao Huang, Storm Mathisen, Rosa Letizia, and Claudio Paoloni are with Engineering Department, Lancaster University, Lancaster, LA1 4YW, UK (e-mail: Xiang.Li@dynexsemi.com; huangxuejiao1987@gmail.com; s.mathisen@lancaster.ac.uk; r.letizia@lancaster.ac.uk; c.paoloni@lancaster.ac.uk). The work has been partially sponsored by EPSRC grant EP/P015883/1.

In this paper, the design and initial fabrication of a 71-76 GHz TWT, using the Double Corrugated Waveguide, as downlink amplifier for high data rate W-band satellite communications is presented. The design is aimed at easing manufacturing and alignment while maximizing the beam–wave interaction. The TWT is designed with two sections separated by a sever for avoiding self-excited oscillations. About 70 W output power is obtained with more than 28 dB gain in the whole frequency band. The DCW electrical behavior was experimentally validated by cold test.

TABLE I
DIMENSIONS OF THE DCW FOR THE 71 – 76 GHZ TWT

	Designed Value (μm)		Designed Value (μm)
a	1700	*p*	1100
b	1270	*r*	160
d	600	*s*	850
g	400	*w*	250
h	680		

The paper is organized as follows: Section II presents the design and cold analysis of the DCW SWS for the 71-76 GHz TWT, Section III focuses on the hot simulation of the complete two sections DCW TWT and Section IV reports on the fabrication and cold test results of the DCW.

II. Double Corrugated Waveguide Design

The DCW was designed to work in forward wave mode in the 71- 76 GHz band [17]. The electron beam specifications are 160 μm radius and 12.3 kV beam voltage. The beam current is set to use a low cathode loading for long life time, compatible with satellite system specifications. The dimensions of the DCW are listed in TABLE I. The distance *g* between the two rows of pillars has been optimized for the best interaction for the given beam radius. The distance of the beam from the metal walls (*g*/2-*r*) is fixed at 40 μm, to assure a good alignment and the highest beam transmission. A specific effort was devoted to minimize the impact of the couplers in the transition between the DCW and the input/output standard WR10 waveguide. The height *b* of the DCW is fixed at 1270 μm to be compatible with the height of the WR10 flange (2540 μm x 1270 μm) and reduce the fabrication steps.

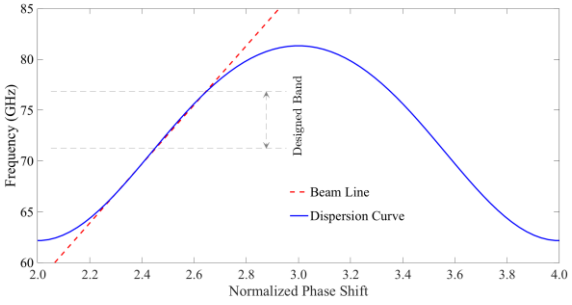

Fig. 2. Dispersion diagram of the DCW with dimension in TABLE I. The beam line at 12.3 kV is superimposed in red.

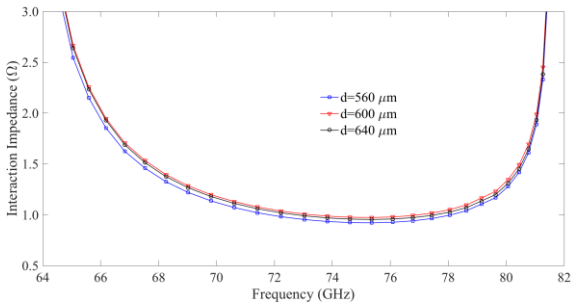

Fig. 3. Variation of the averaged interaction impedance of the DCW as a function of the beam position *d*.

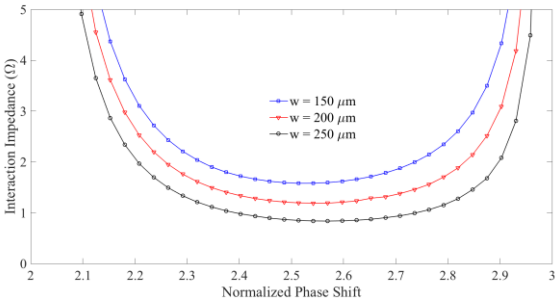

Fig. 4. Averaged interaction impedance as a function of the pillar section *w*.

The beam-wave interaction is set in the forward wave region of the first space harmonic, to obtain broadband synchronization at a low beam voltage. The dispersion curve of the DCW, calculated by the eigenmode solver of CST Microwave Studio [19], with superimposed 12.3 kV electron beam line, is shown in Fig. 2. A very good beam-wave synchronization has been obtained in the 71-76 GHz frequency band.

The vertical position *d* of the beam is chosen to maximize the averaged interaction impedance on the circular cross-section of the electron beam. The interaction impedance for different axis position *d* of the electron beam is shown in Fig. 3. The optimum value d = 600 μm is assumed in the following, that ensures an averaged interaction impedance of about 1 Ω in the operation frequency range, sufficient to support adequate energy transfer from the electron beam to the propagating wave. A substantial improvement of the interaction impedance can be obtained reducing the pillar cross section *w*. Fig. 4 shows the interaction impedance as a function of the phase shift for three values of *w*. An increment of 100% is obtained when reducing the pillar dimension by 100 μm (w = 150 μm).

III. Fabrication and Cold Test

The dispersion curve of the DCW has been experimentally validated following the process illustrated in [20]. Two identical test DCWs were realized by conventional CNC milling in Aluminum (Fig. 5) with 10 periods and 20 periods respectively.

The DCW dimensions listed in TABLE I were used. To simplify the fabrication, linear couplers tapered in height are adopted to connect the WR-10 flanges. Each coupler has 15 pillar pairs with the height linearly tapered from the nominal

height of 640 μm down to 80 μm. Each DCW was fabricated in two parts: a bottom flat part with all the pillars and a top part with the waveguide and the electron beam tunnel. This fabrication approach reduces the CNC milling effort and allows the use of tooling with large diameter. It is noteworthy that the assembly of the two parts needs only alignment pins and screws. Fig. 5 shows the fabricated top and bottom parts and the pillar profile. Before the assembly, the two parts were cleaned by acetone and ultrasound to remove metal residues. The microscopic view of the fabricated pillars is shown in Fig. 6.

The S-parameters of the fabricated DCWs were measured by Rohde&Schwarz Vector Network Analyzer with millimeter wave extension at W-band. The S-parameters of the 10-periods

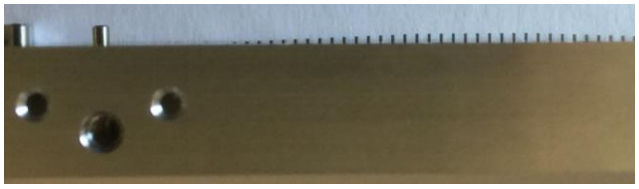

a)

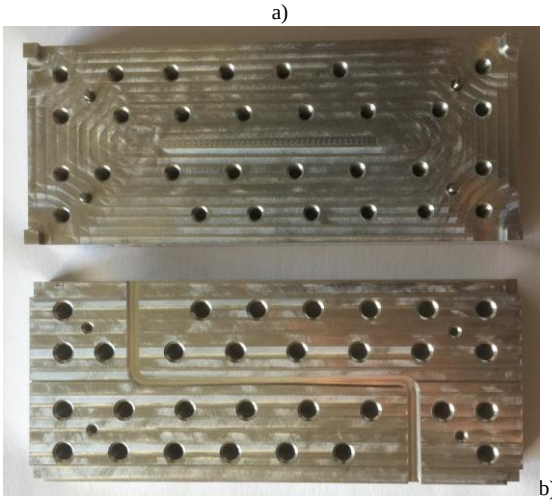

b)

Fig. 5. The fabricated DCW SWS. (a) Side view of the pillars; (b) Top view of the fabricated top and bottom parts.

DCW are shown in Fig. 7. The measured S_{21} is lower than the simulated value. This can be explained by the relatively low electric conductivity at the interface between the two parts and a slightly irregular surface flatness caused by the vibration of toolings during the CNC fabrication process. However, the good agreement demonstrates that the tolerance of a few microns typical of an affordable CNC milling process have a limited effect on performance. The fabrication of the DCW for the final TWT will be done in copper and the two parts will be joined by diffusion bonding. An identical DCW with 20 periods has been also fabricated in Aluminum. The S-parameters were measured, with the purpose to obtain the phase of the transmitted signal. The dispersion curve of the DCW has been derived by the difference of the measured phases of the transmitted signals of the 10 periods and the 20 periods DCWs. The phase difference is given by:

$$\Delta\varphi(f) / \Delta L = \beta(f) \cdot p \qquad (1)$$

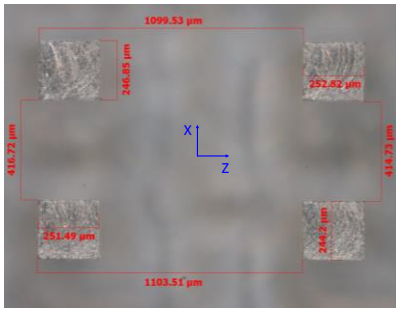

Fig.6. Detailed view of the fabricated pillars of the DCW.

where $\Delta\varphi(f)$ is the phase difference as a function of frequency f, ΔL is the DCW length difference, $\beta(f)$ is the propagation constant and p is the period of the DCW [20]. The experimental and simulated dispersion curves of the DCW are shown in Fig. 8. It can be observed the very good agreement in the operation frequency band. The difference at the lower band edge is mainly

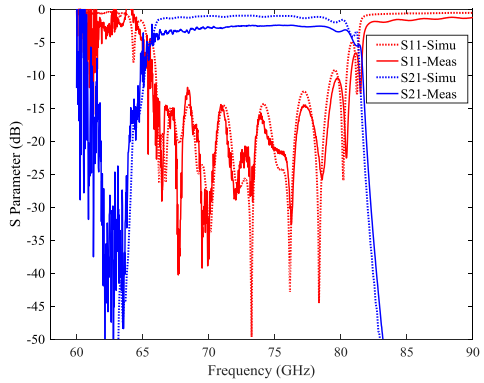

Fig. 7. Comparison between the simulated and measured S parameters for the 10 periods DCW with linear taper.

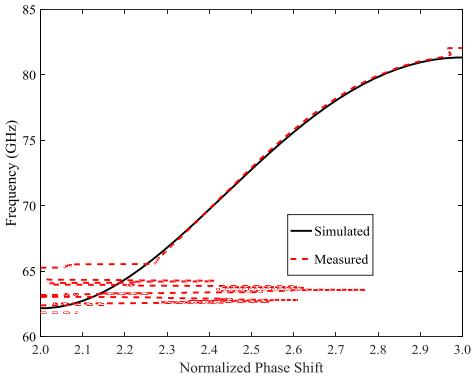

Fig. 8. Comparison between the simulated and measured dispersion curve of the fabricated DCW.

caused by the use of the W-band converters at the limit of their band, below 66 GHz. Consequently, the results are seriously affected by the phase distortion and extremely low signal-noise ratio. The difference at the upper band edge is mainly caused by fabrication tolerances.

IV. Hot Simulations

The large signal performance of the DCW TWT is investigated via 3D Particle in Cell (PIC) simulations performed by CST Particle Studio on a workstation with GPU NVIDIA K40. An electron beam with voltage of 12.8 kV, beam current of 100 mA and 160 μm radius is considered. The electron beam voltage in the hot simulation is optimized to maintain satisfying beam-wave interaction and thus it is slightly higher than the value predicted by cold analysis. The focusing magnetic field is set as 0.3 T. The conductivity of the copper is reduced to $\sigma = 2.353\times10^7$ S/m to account for eventual ohmic losses due to surface roughness. The input power at Port 1 is 100 mW. This value is compatible with solid state power amplifiers available in the market. A first set of simulations was performed to evaluate the performance of a single section TWT with 80 periods, as a function of the pillar cross section, with all the other dimensions fixed. This study permitted to verify the effect of the improvement of the interaction impedance due to the reduction of the pillar section reported in Fig.4. Fig. 9 shows that more than 6 dB gain and 40 W output power increase is obtained by reducing the pillar dimensions.

V. DCW TWT Design

The 71-76 GHz DCW TWT is made of two sections with 40 and 80 periods of uniform pillars, respectively, separated by a sever. This is a typical two-section configuration to suppress the self-excitation and achieve high gain. The dimensions of the pillars are the same as in Table I, to evaluate the full TWT performance in the conservative case of pillars with w =250 μm. The two sections are connected by an electron beam tunnel which is cut-off at W-band. Each end of the DCW is connected

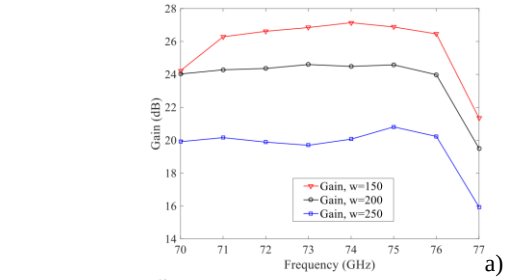

a)

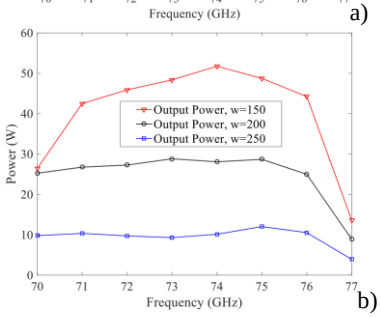

b)

c)

Fig. 9. a) Gain, b) output power for 80 periods single section TWT as a function of the pillar section, c) simulation setup.

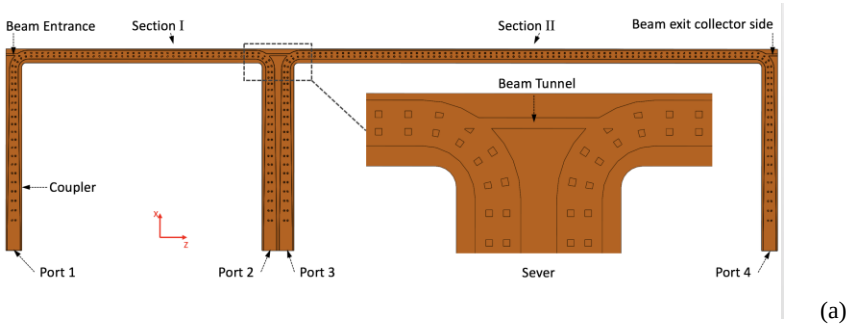

(a)

(b)

Fig.10. Section view of the full DCW TWT interaction structure a) top view, b) coupler side view.

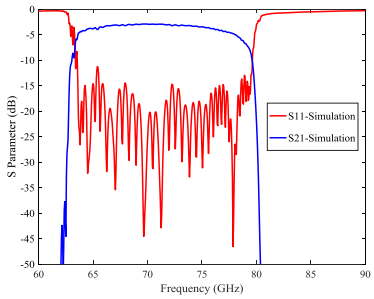

Fig. 11. Simulated S-parameters of Section I of the DCW TWT

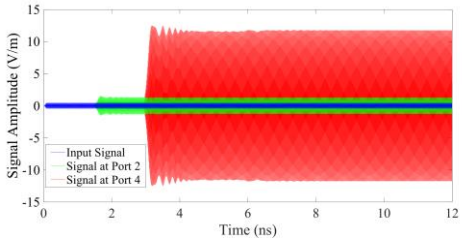

Fig. 12. Input and output signal variation in time for the DCW TWT at 71 GHz.

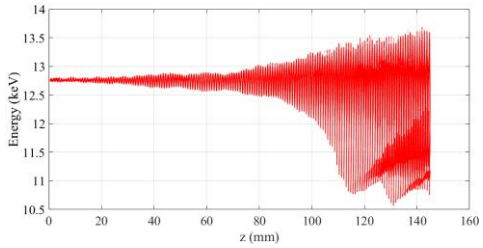

Fig. 13. Electron energy distribution as a function of the axial distance for the DCW TWT.

to the flange by a coupler connected to a 90-degree DCW bend. The use of the bent DCW permits to reduce significantly the length of the SWS and thus the focusing magnet, removing from the interaction zone the tapered region of the DCW, to couple the TE_{10} to the DCW mode. Each coupler comprises 18 pillar pairs tapered in height and 6 pillars with nominal height. The configuration of the height-tapered pillar pairs is shown in Fig. 10 (b). The four pillar pairs in the bend region before the coupler are shaped and optimized to provide good transmission property, easy manufacturability and sufficient distance from the electron beam. The length of the whole structure in the *z* direction is about 145 mm.

The input power signal is injected in Port 1 of Section I and propagates towards Port 2, modulating the electron beam current. The slightly amplified wave is then absorbed in Port 2 to avoid reflections, by high-loss material (graphite). The modulated electron beam travels into Section II, where by a longer interaction DCW section, the signal is amplified to the specification values at Port 4. The small portion of reflected power in Port 3 will be also absorbed by high-loss absorbing materials.

The optimization of the DCW bend and the coupler was carried out by CST Microwave Studio [19]. Fig. 11 shows the simulated S-parameters of Section I (Port 1 to Port 2) that includes two DCW bends and two couplers, assuming a reduced

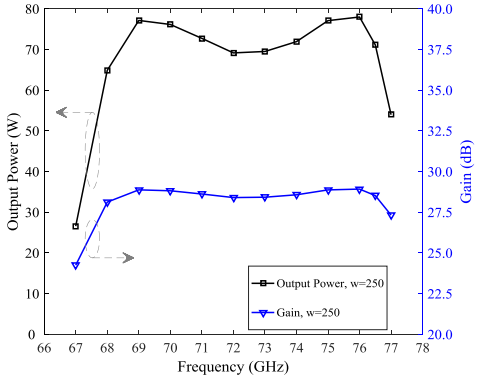

Fig.14. Output power and gain of the DCW TWT.

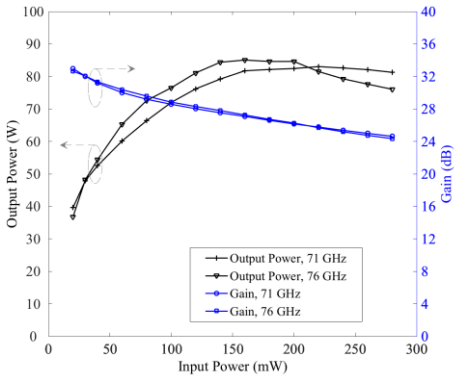

Fig.15. Output power as a function of the input power at 71 GHz and 76 GHz.

copper conductivity $\sigma = 2.353\times10^7$ S/m to take into account the finite surface roughness of the fabricated DCW. The S_{11} is better than -14.7 dB in the frequency band. The S_{21} is around -4 dB having conservatively assumed high copper ohmic loss. In this simulation, the electron beam, generated by a conventional Pierce gun, has 12.8 kV voltage, 150 mA current and radius of 160 μm. The higher current was used to increase the gain due to the use of pillars with w = 250 μm. The focusing magnetic field is set as 0.3 T. The input power at Port 1 is 100 mW.

Fig. 12 shows the instantaneous signal amplitude at Port 1, Port 2 and Port 4 at 71 GHz. The signal at Port 2 starts to grow earlier than at Port 4 as expected. The gain achieved at Port 2 is about 8 dB due to the low beam-wave energy interaction resulting from the short DCW length. The output power at the output Port 4 stabilizes at about 4 ns producing 72.7 W power. The output signals at Port 1 and 3 are negligible, demonstrating the good matching of the couplers. The electrons energy distribution in the axial direction (Fig. 13) shows a strong modulation of the electron beam in the second section of the TWT, where most of the electrons lose energy in favor of the wave.

Output power and gain in the 71-76 GHz frequency band are shown in Fig. 14. The output power varies from 69 to 79 W, with output power levels at the frequency band edges higher than those at the center. This can be explained by the variation of the synchronization condition and interaction impedance across the band. A flat gain of about 28.5 dB is demonstrated.

The output power and gain variation of the DCW TWT as a

function of the input power, at 71 GHz and 76 GHz, is shown in Fig. 15. The output power increases at the increase of input power from 40 to 140 mW, showing the expected saturation for higher input power. The output gain reduces at the increase of the input power.

VI. Conclusion

A 71-76 GHz DCW TWT has been designed for high data rate satellite communication downlink. Output power of about 70 W and 28 dB gain across the frequency band have been demonstrated. The good performance, simple fabrication by CNC milling, easy assembly and robustness to tolerances make the Double Corrugated Waveguide a suitable SWS for space millimeter wave tubes to enable W-band high capacity communication satellites. The DCW has been experimentally validated by the good agreement of the S-parameters and the dispersion curve with the simulations. The presented DCW TWT design is also a test vehicle at scaled frequency for using the same topology for a 220 GHz TWT for high capacity wireless networks for terrestrial applications.

References

[1] Cisco Visual Networking Index: Global Mobile Data Traffic Forecast Update, 2016–2021 (2017). [Online]. http://www.cisco.com/c/en/us/solutions/collateral/service-provider/visual-networking-index-vni/mobile-white-paper-c11-520862.pdf.

[2] A. Jebril, M. Lucente, M. Ruggieri, and T. Rossi, "WAVE-a new satellite mission in W-band," in *Proc. IEEE Aerospace Conf.*, Big Sky, MT, USA, Mar. 2005, pp. 870-879.

[3] M. De Sanctis, E. Cianca, T. Rossi, C. Sacchi, L. Mucchi, and R. Prasad, "Waveform design solutions for EHF broadband satellite communications," *IEEE Commun. Mag.*, vol. 53, no. 3, pp. 18-23, 2015.

[4] P. A. N. Ayllon, M. Ludwig, R. Dionisio, "An overview of European Spaceborne Vacuum Tube Amplifiers and System Needs," in *Proc. IEEE 18th Int. Vac. Electron. Conf.*, London, UK, April. 2017, p. 12.

[5] R. Acosta, J. Nessel, R. Simons, M. Zemba, J. Morse, and J. Budginer, "W/V-Band RF Propagation Experiment Design," 18th Ka and Broadband Communication Conference, Ottawa, Canada, Sept 2012.

[6] U. Lewark, J. Antes, J. Walheim, J. Timmermann, T. Zwick, and I. Kallfass, "Link budget analysis for future E-band gigabit satellite communication links (71–76 and 81–84 Ghz)," *CEAS Space J.*, vol. 4, no. 1-4, pp. 41-46, 2013.

[7] M. Koker, E. Watkins, and N. Deo, "High power Solid-State Power Amplifiers for airborne and space applications in remote sensing and communications," in *Proc. Asia-Pacific Microwave Conf.*, Tokyo, Japan, Nov. 2014, pp. 579-581.

[8] C. K. Chong and W. L. Menninger, "Latest advancements in high-power millimeter-wave helix TWTs," *IEEE Trans. Plasma Sci.*, vol. 38, no. 6, pp. 1227-1238, 2010.

[9] N. R. Robbins, D. R. Dibb, and W. L. Menninger, "mm-Wave space helix TWT performance and experience," in *Proc. IEEE 14th Int. Vac. Electron. Conf.*, April. 2013.

[10] N. R. Robbins, D. R. Dibb, and W. L.Menninger, "Space qualified, 75-watt V-band helix TWTA," in *Proc. IEEE 13th Int. Vac. Electron. Conf.*, April. 2012.

[11] B. Qu, X. Liang, J. Feng, G. Yan, C. Guo, Y. Shang, "Development of Millimeter-wave Space TWTs in BVERI" in *Proc. IEEE 18th Int. Vac. Electron. Conf.*, April. 2017.

[12] S. Sengele, H. Jiang, J. H. Booske, C. L. Kory, D. W. Van der Weide, and R. L. Ives, "Microfabrication and characterization of a selectively metallized W-band meander-line TWT circuit," *IEEE Trans. Electron Devices*, vol. 56, no. 5, pp. 730-737, 2009.

[13] C. Chua, J. M. Tsai, S. Aditya, M. Tang, S. W. Ho, Z. Shen, and L. Wang, "Microfabrication and characterization of W-band planar helix slow-wave structure with straight-edge connections," *IEEE Trans. Electron Devices*, vol. 58, no. 11, pp. 4098-4105, 2011.

[14] A. Baig, D. Gamzina, T. Kimura, J. Atkinson, C. Domier, B. Popovic, L. Himes, R. Barchfeld, M. Field, and N. C. Luhmann, "Performance of a Nano-CNC Machined 220-GHz Traveling Wave Tube Amplifier," *IEEE Trans. Electron Devices*, vol. 64, no. 5, pp. 2390-2397, 2017.

[15] C. D. Joye, A. M. Cook, J. P. Calame, D. K. Abe, A. N. Vlasov, I. A. Chernyavskiy, K. T. Nguyen, E. L. Wright, D. E. Pershing, and T. Kimura, "Demonstration of a high power, wideband 220-GHz traveling wave amplifier fabricated by UV-LIGA," *IEEE Trans. Electron Devices*, vol. 61, no. 6, pp. 1672-1678, 2014.

[16] M. Mineo and C. Paoloni, "Double-corrugated rectangular waveguide slow-wave structure for terahertz vacuum devices," *IEEE Trans. Electron Devices*, vol. 57, no. 11, pp. 3169-3175, 2010.

[17] Xiang Li, Xuejiao Huang, Rosa Letizia, Claudio Paoloni, "71-76 GHz Traveling Wave Tube for High Data Rate Satellite Communication," in *Proc. IEEE 18th Int. Vac. Electron. Conf.*, London, UK, April. 2017.

[18] A. Malekabadi, and C. Paoloni. "UV-LIGA microfabrication process for sub-terahertz waveguides utilizing multiple layered SU-8 photoresist." *Journal of Micromechanics and Microengineering*, vol. 26, 095010, 2016.

[19] CST Studio Suite Help Document, CST Corp., Darmstadt, Germany. (2016). [Online]. Available: http://www.cst.com/.

[20] C. Paoloni, M. Mineo, M. Henry, and P. G. Huggard, "Double corrugated waveguide for ka-band traveling wave tube," *IEEE Trans. Electron Devices*, vol. 62, no. 11, pp. 3851-3856, 2015.

Xiang Li received the B.S. degree in vacuum electronics technology from the University of Electronic Science and Technology of China, Chengdu, China, in 2009, and the Ph.D. degree in electronic engineering from the Queen Mary University of London, London, U.K. in 2016. In 2016, he joined Lancaster University, Lancaster, U.K., as a research associate in vacuum electronic devices.

Xuejiao Huang received the B.S. degree in urban underground space engineering from the Central South University, Changsha, China, in 2010, and the Ph.D. degree in Aerospace Engineering from the Queen Mary University of London, London, U.K. in 2016. In 2016, she joined Lancaster University, Lancaster, U.K., as a research associate in vacuum electronic devices.

.

Storm Mathisen received the BEng (Hons) Aerospace Engineering with Year in Industry degree from the Swansea University, Swansea, United Kingdom, in 2016. He is currently working as PhD student in microfabrication processes for millimeter wave vacuum devices at Engineering Department, Lancaster University, UK.

Rosa Letizia (M'13) received the Laurea degree in Electronic Engineering from the Polytechnic of Bari, Bari, Italy and the Ph.D. degree in computational photonics from the University of Leeds, Leeds, U.K., in 2005 and 2009, respectively. Since 2011, she has been a Lecturer at the Engineering Department, Lancaster University, U.K., and with the Cockcroft Institute, Warrington, U.K.

Claudio Paoloni (M'86–SM'11) received the Laurea Degree in Electronic Engineering from the University of Rome "Sapienza", Rome, Italy, in 1984. Since 2012, he has been a Professor of Electronics with the Department of Engineering, Lancaster University, Lancaster, U.K. Since 2015, he has been the Head of Engineering Department. He is Chair of the IEEE EDS Vacuum Electronics Technical Committee.